Supporting Information for "Observational evidence of the excitation of magnetosonic waves by an He^{++} ion ring distribution"

S. G. Claudepierre[1,2], X. Liu[3], L. Chen[3], and K. Takahashi[4]

[1]Space Sciences Department, The Aerospace Corporation, El Segundo, California, USA

[2]Department of Atmospheric and Oceanic Sciences, UCLA, Los Angeles, California, USA

[3]Department of Physics, University of Texas at Dallas, Richardson, TX, USA

[4]The Johns Hopkins University Applied Physics Laboratory, Laurel, Maryland, USA

Contents of this file

   1. Text S1 to S4

   2. Figures S1 to S9

Introduction

   This document provides additional analysis to support the interpretations presented in the main manuscript. Section S1 describes additional solar wind measurements that are used to fill gaps in the OMNI data. Section S2 provides additional evidence that the helium injections observed by RBSPICE are doubly-ionized, rather than-singly ionized, helium ions. Section S3 presents an analysis of observed ULF waves that are used to infer the average ion mass during the MS wave event. Finally, Section S4 presents figures

———

May 3, 2021, 9:39pm

18 showing the ion measurements from Probe B and for the ion species not shown in the

19 main manuscript.

Text S1: Solar Wind Measurements

As noted in the main manuscript, there are gaps in the 5-minute OMNI data during the MS wave event. We filled in these gaps using the WIND measurements shown in Figure S1, which were averaged onto the same time cadence as the OMNI data. The good agreement amongst the various data sources shown in Figure S1 validates this gap-filling procedure. We note that a shock impacted the magnetosphere on Feb-07 at 16:16:00 UTC, well before the MS wave event under investigation. This is identified as a fast forward shock in the online database of interplanetary shocks observed by WIND that is maintained by the Harvard & Smithsonian Center for Astrophysics at `https://lweb.cfa.harvard.edu/` `shocks/`.

Text S2: Singly- vs Doubly-Ionized Ion Injections

As illustrated in Mitchell, Gkioulidou, and Ukhorskiy (2018), ion injections in the RB-SPICE energy range very often exhibit energy dispersion features that indicate the presence of higher-charge state ions. Specifically, they demonstrated that many injections observed in the RBSPICE channels have both singly- and doubly-ionized ion injection signatures simultaneously for a single, isolated injection. The telltale sign for singly- and doubly-ionized ions is the presence of an energy-dispersed injection feature in the energy-time spectrogram accompanied by a similar feature at twice the energy at the same time (c.f., their Figure 1). This is the result of the energization processes at work during the injection. Ions with different charge states will be subjected to different rates of energization (via the convective electric field) and follow different drift paths while conserving their 1st adiabatic invariant. Specifically, a charged particle will gain energy when transported in the direction of the electric field as $\Delta W \sim qEd$. Here, q is the charge state, E is

the roughly constant convection electric field strength, and d is the distance the particle moves parallel to the electric field. A doubly-ionized ion will thus gain roughly twice the energy as a singly-ionized ion (i.e., by a factor proportional to the ratio between the two charge states).

Mitchell et al. (2018) performed a detailed cross-correlation analysis on the RBSPICE energy channels for various pairs of species and assumed charge states. We present an analysis here in a similar spirit, though we note that the injection signatures in the MS wave event are not nearly as strong and coherent as theirs, since the ions have dispersed considerably by the time they reach the spacecraft in the present case. Figure S2 shows time series of RBSPICE helium ions in grey, and protons in magenta and green for the entire Probe A orbit in question. We separate the orbit into two time intervals, t_1 and t_2. The MS wave event interval is indicated by the horizontal orange bar labeled t_2. The remainder of the orbit is indicated by the horizontal blue bar labeled t_1. The energy-dispersed injection that leads to the helium ion ring distribution noted in the main manuscript appears in panels (b)-(d) as the peak in ion flux just prior to 00:50:00 UTC (i.e., during the t_2 interval).

In panels (b)-(d), two RBSPICE proton channels are shown, one at roughly the same energy as the helium channel shown and one at roughly half the energy. In panel (b), we see that the grey and the magenta traces closely track one another in time during the t_1 portion of the orbit and begin to diverge in the t_2 interval. Since these two time series are of protons and helium ions at the same energy, their close correlation during the beginning portion of the interval suggests that the helium ions are singly ionized. To further quantify this relationship, we compute the cross-correlation coefficients between

May 3, 2021, 9:39pm

66 the helium channel and the two protons channels during the t_1 interval, labeled as r_1 in

67 the figure. Here, we see a high correlation (0.87) between the helium and proton channels

68 at the same energy, and a lower correlation (0.35) between the helium channel and the

69 proton channel at half the energy.

70 An analogous set of correlations coefficients is computed during the t_2 interval and

71 labeled as r_2 in the figure. Note that during this later portion of the orbit, the correlation

72 is in the opposite sense. We now see a high correlation between the helium channel and

73 the proton channel at half the energy, and a lower correlation between the helium and

74 proton channels at the same energy. This suggests that during the t_2 interval, the helium

75 ions are doubly ionized. Overall in panels (b)-(d), we find a high degree of correlation

76 between the grey and green traces during the t_2 interval, which suggests that the ions

77 reported in the RBSPICE helium channel are doubly ionized (He^{++}) during this time

78 and at these energies. This is in accordance with one of the main findings of Mitchell et

79 al. (2018), that He^{++} dominates the helium charge state for plasma recently transported

80 from higher L during an injection. Note that in panel (a), while a corresponding proton

81 channel is not available from RBSPICE at half the energy, the same relationship holds

82 between the helium and proton channels at the same energy (i.e., a high correlation in t_1

83 and a lower correlation in t_2).

84 It is not possible to use the HOPE measurements at lower energy for this type of analysis.

85 A careful consideration of the HOPE time-of-flight matrix in Funsten et al. (2013) (their

86 Figure 35) reveals that doubly ionized helium in fact shows up in the HOPE proton

87 channel, due to the action of the electrostatic analyzer. This effect is most pronounced at

88 the higher HOPE energies of interest here (1-50 keV) and is discussed in greater detail in

89 Vira, Larsen, Skoug, and Fernandes (2021) (c.f., their Figure 9).

90 **Text S3: ULF Wave Magnetoseismology**

91 Ultra-low frequency (ULF) waves observed during the MS wave event can provide an

92 independent estimate of the average ion mass during the event. Figure S3 shows an

93 overview of ULF wave activity for the entire Van Allen Probe A orbit that encompasses the

94 MS wave event. The spacecraft magnetic coordinates are defined using a centered dipole

95 with the Gauss coefficients taken from IGRF. As described by Takahashi and Denton

96 (2021), the spectral parameters shown in this figure were obtained using a 15-min data

97 window and moving it forward in 5-min steps. Around the time of the event ($\sim$00:00:00 -

98 02:00:00 UTC), the fundamental (T1) and third harmonic (T3) toroidal mode ULF waves

99 are clearly seen in panels (b)-(d), which display spectral parameters associated with the

100 azimuthal component of the magnetic field. The T1 and T3 harmonic mode numbers

101 can be unambiguously determined by comparing theoretical calculations of standing wave

102 mode structures and the observed cross-phase values of these waves, which remained near

103 -90 degrees (blue) as the spacecraft moved slightly south of the magnetic equator (MLAT

104 < 0).

105 The observed frequency of the third harmonic standing wave (f_{T3}) is shown in Figure S4a

106 for the inbound leg of the orbit shown in Figure S3. We convert this frequency to the

107 mass density as described in Takahashi et al. (2015). The results are shown in panel (b)

108 along with the electron density. The analysis was done using a 15-min data window and

109 moving it forward in 5-min steps. During the time of the MS wave event at 00:00:00 -

110 02:00:00 UTC, the electron density and mass density values are very close to one another

111 (panel (b)), and as a consequence, the inferred average ion mass value is very close to 1

112 amu (panel (c)). This suggests that the cold plasma is dominated by protons at this time,

113 which is typical inside of the plasmasphere. We note that these results depend on the

114 assumed models for the background magnetic field and the field line mass distribution, as

115 discussed in Takahashi et al. (2015).

Text S4: Additional Ion Flux Measurements

117 Figure S5 and Figure S6 show the proton and oxygen ion PSD measurements from

118 Van Allen Probe A in an analogous format to the helium figure from the manuscript.

119 Figure S7, Figure S8, and Figure S9 show the proton, helium, and oxygen ion PSD from

120 Van Allen Probe B in the same format.

References

121 Funsten, H. O., Skoug, R. M., Guthrie, A. A., MacDonald, E. A., Baldonado, J. R.,

122 Harper, R. W., ... Chen, J. (2013, November). Helium, Oxygen, Proton, and

123 Electron (HOPE) Mass Spectrometer for the Radiation Belt Storm Probes Mission.

124 *Space Sci. Rev.*, *179*, 423-484. doi: 10.1007/s11214-013-9968-7

125 Mitchell, D. G., Gkioulidou, M., & Ukhorskiy, A. Y. (2018, August). Energetic Ion

126 Injections Inside Geosynchronous Orbit: Convection- and Drift-Dominated, Charge-

127 Dependent Adiabatic Energization (W = qEd). *J. Geophys. Res.*, *123*(8), 6360-6382.

128 doi: 10.1029/2018JA025556

129 Takahashi, K., & Denton, R. E. (2021, n/a). Nodal structure of toroidal standing alfvén

130 waves and its implication for field line mass density distribution. *J. Geophys. Res.*,

131 *n/a*(n/a), e2020JA028981. doi: 10.1029/2020JA028981

132 Takahashi, K., Denton, R. E., Kurth, W., Kletzing, C., Wygant, J., Bonnell, J., ...
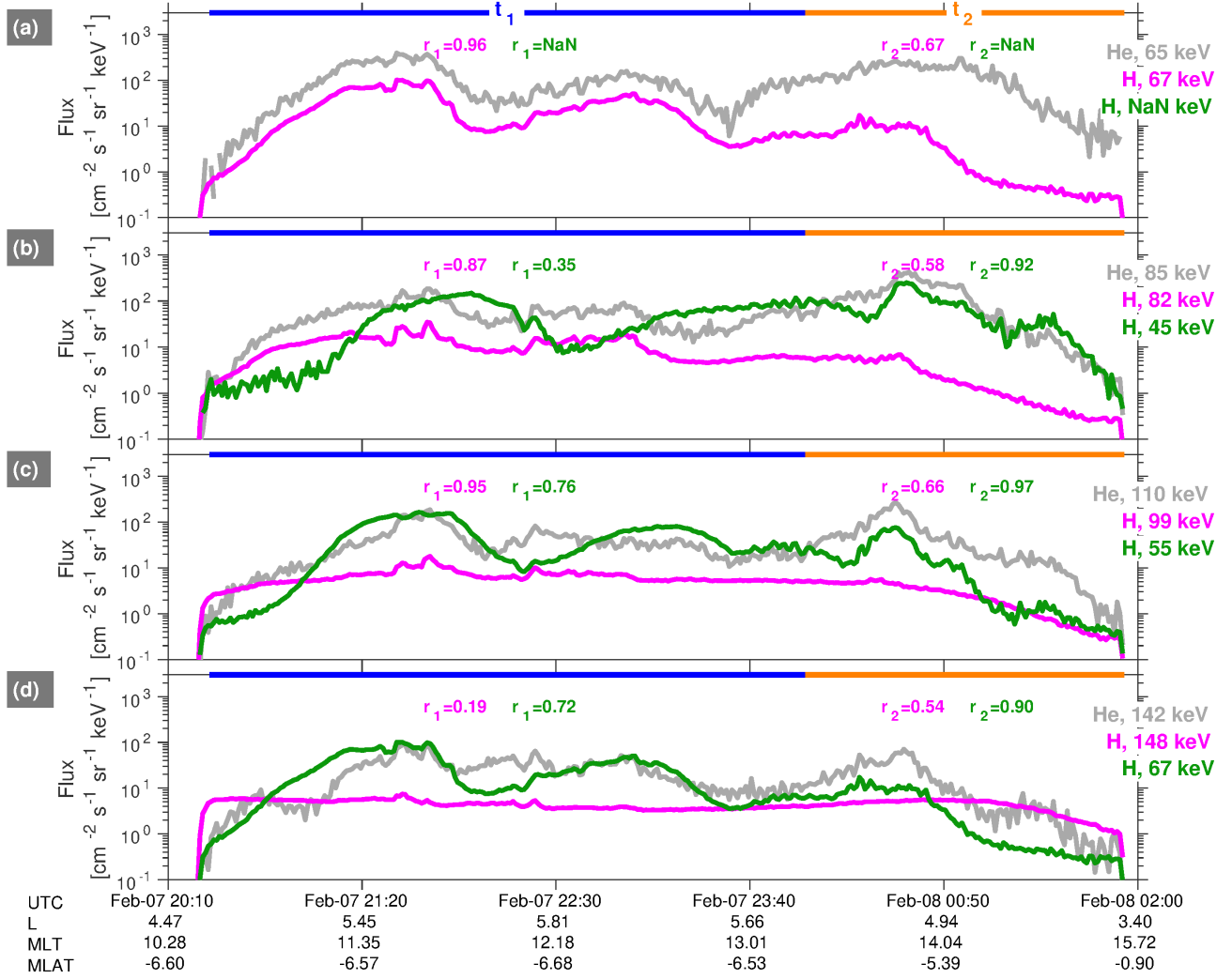
133 MacDowall, R. (2015, January). Externally driven plasmaspheric ULF waves

134 observed by the Van Allen Probes. *J. Geophys. Res.*, *120*(1), 526-552. doi:

135 10.1002/2014JA020373

136 Vira, A. D., Larsen, B. A., Skoug, R. M., & Fernandes, P. A. (2021). Bayesian

137 model for hope mass spectrometers on van allen probes. *J. Geophys. Res.*, *126*(3),
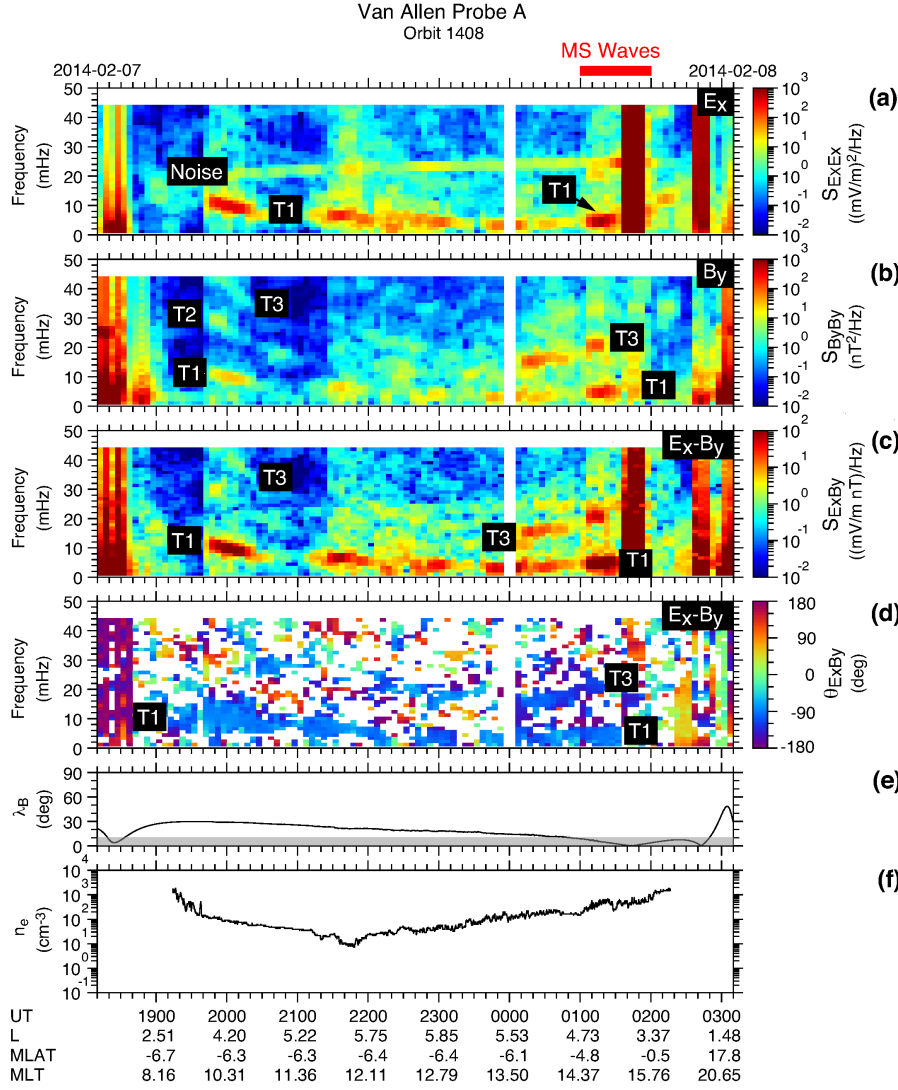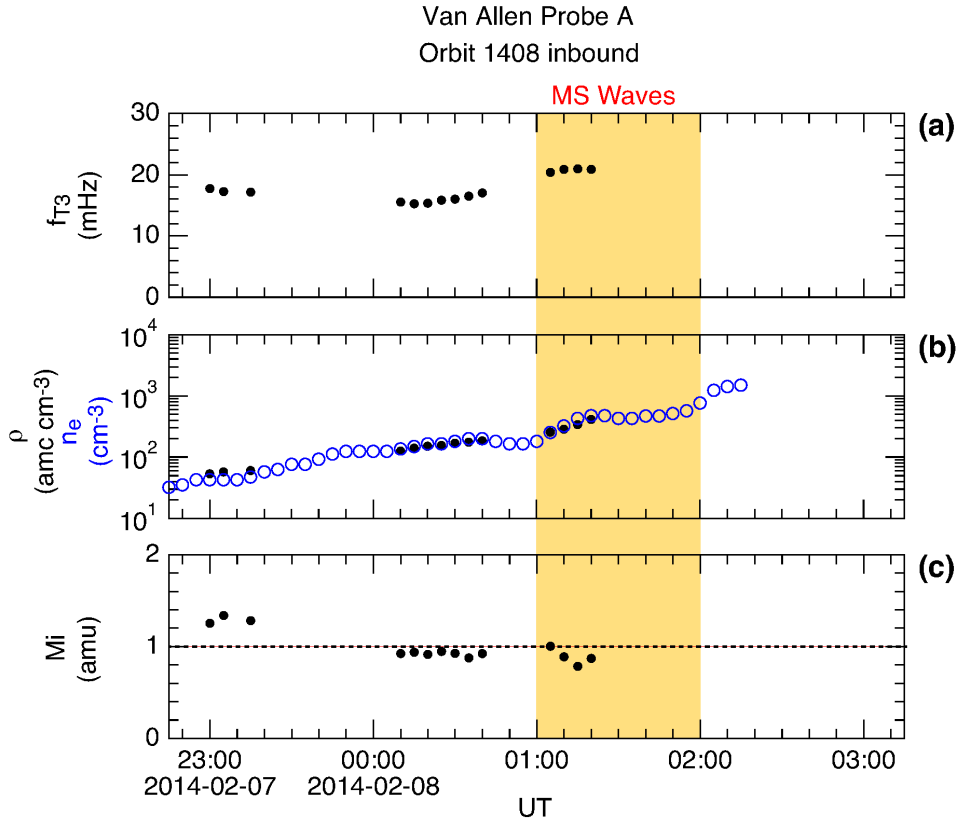
138 e2020JA028862. doi: 10.1029/2020JA028862

Figure S1. Solar wind measurements from various sources. The top, middle, and bottom panels show the solar wind speed, proton number density, and z-component (GSM) of the interplanetary magnetic field, respectively. There is no magnetic field data from ACE and the ARTEMIS density is the electron density, as there are issues with the proton number density for the dense beam that appears around 00:00 UTC on Feb-08. The ACE and WIND data are time-shifted by 45 minutes. The ARTEMIS-P1 data are not time-shifted as the spacecraft was located just upstream of the bow shock at this time. For the ARTEMIS data, there are two periselene passes through the lunar wake during the displayed time interval. These produce data spikes in the moments and are manually removed in post-processing. Data spikes are also removed from the WIND density and speed measurements using a median filter.
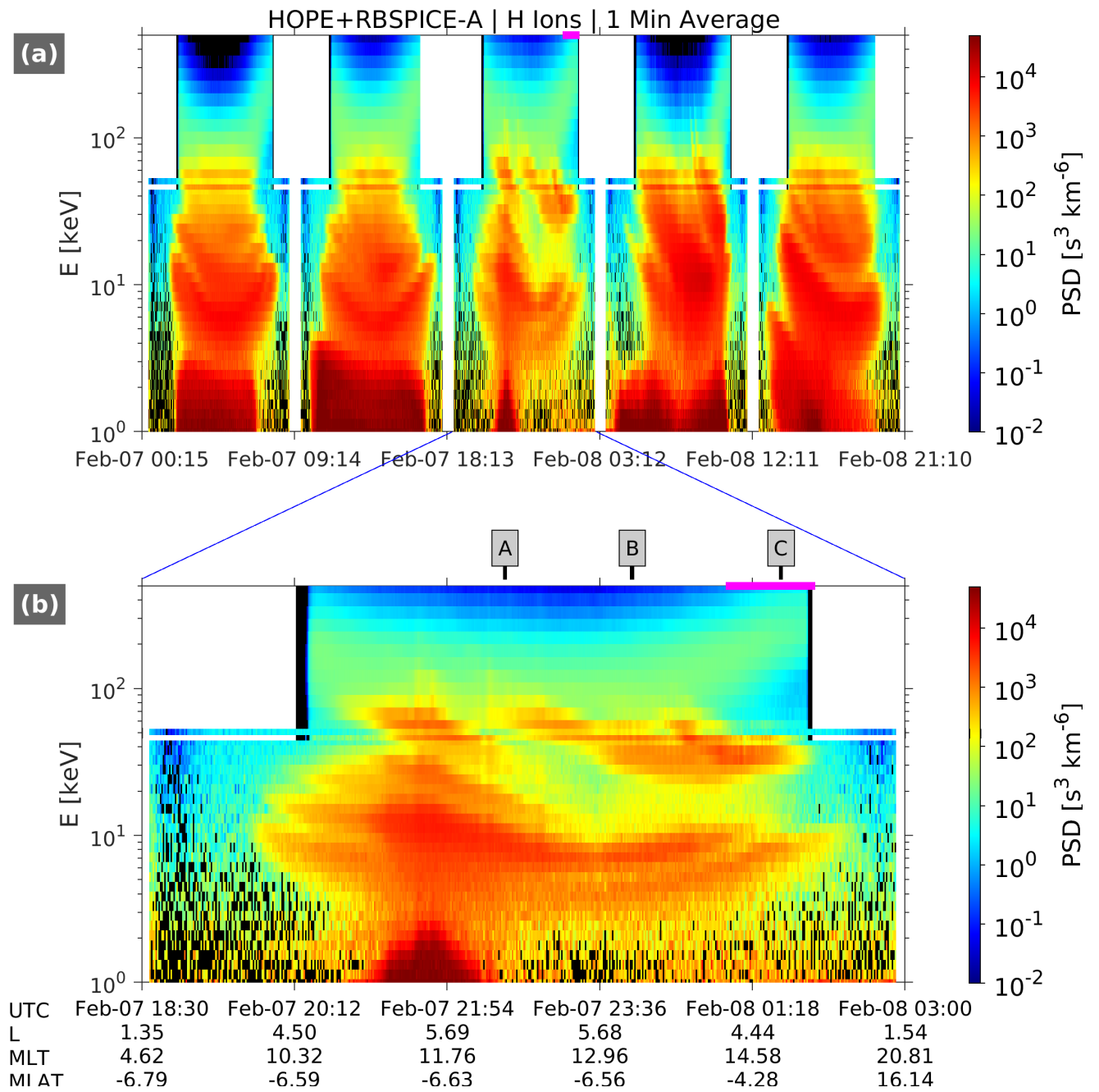
May 3, 2021, 9:39pm

Figure S2. **(a)-(d)** A correlation analysis of RBSPICE helium measurements at fixed energy compared with proton measurements at the same energy and half the energy (see text for details). For fixed ion kinetic energy, W, we note that a high correlation between He(W) and H($W/2$) implies that the ions in the RBSPICE helium channel are He^{++}, while a high correlation between He(W) and H(W) implies that the ions in the RBSPICE helium channel are He^{+}.
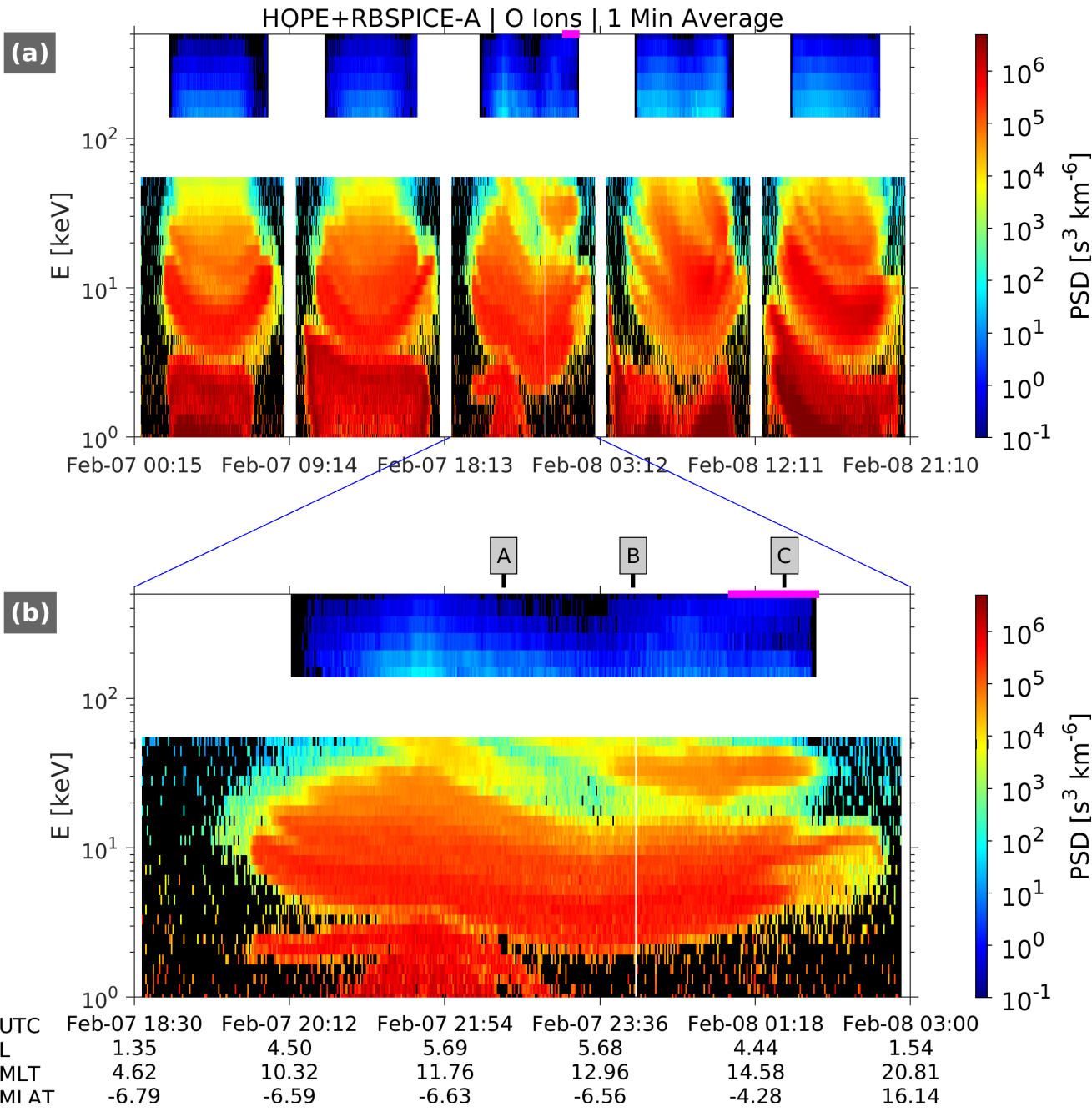
May 3, 2021, 9:39pm

Figure S3. Overview of toroidal mode ULF wave activity observed by Van Allen Probe A on the orbit that include the selected MS wave event (red horizontal bar at the top). **(a)** Power spectra of the radial component of the electric field (E_x) in MFA coordinates. **(b)** Power spectra of the azimuthal component of the magnetic field (B_y). **(c)** E_x-B_y cross-power spectra and **(d)** E_x-B_y cross-phase. **(e)** Magnetic field elevation angle from the spacecraft spin plane. If this angle is low, the spin-axis component of the electric field derived from the measured spin plane components using the assumption $\mathbf{E} \cdot \mathbf{B} = 0$ may contain large errors, which propagate to all components in MFA coordinates. The domain below 10 degrees is shaded as an indicator of potentially large errors of the electric field MFA components. **(f)** Electron density from the EMFISIS upper hybrid line.
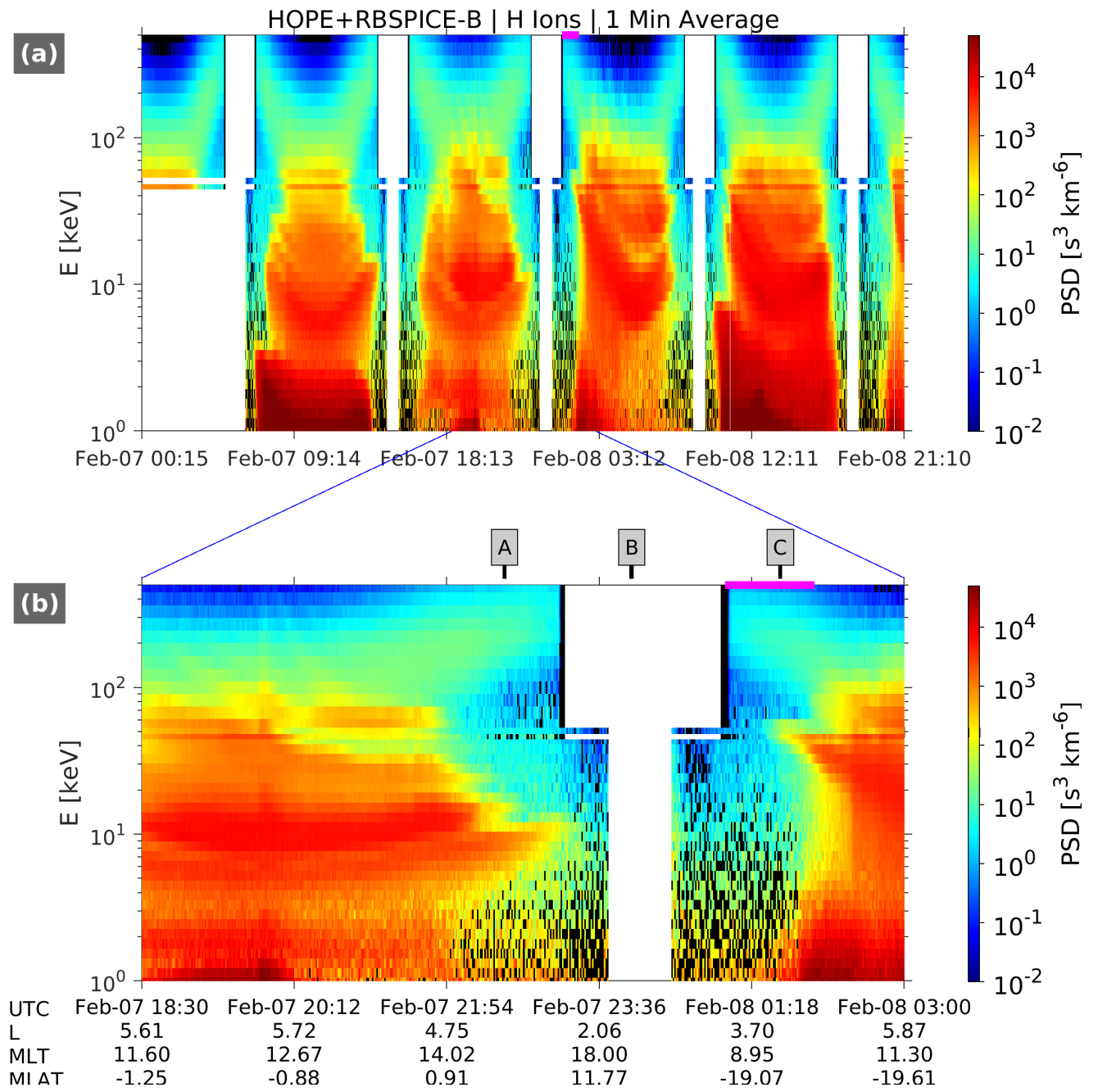
May 3, 2021, 9:39pm

Figure S4. (a) Observed toroidal mode wave frequency in the third harmonic (f_{T3}). (b) The observed electron density (n_e) obtained from EMFISIS and the mass density (ρ) estimated from f_{T3}. (c) Average ion mass Mi ($= \rho/n_e$). Note that $Mi = 1$ (horizontal dashed line) for an all-H$^+$ plasma.
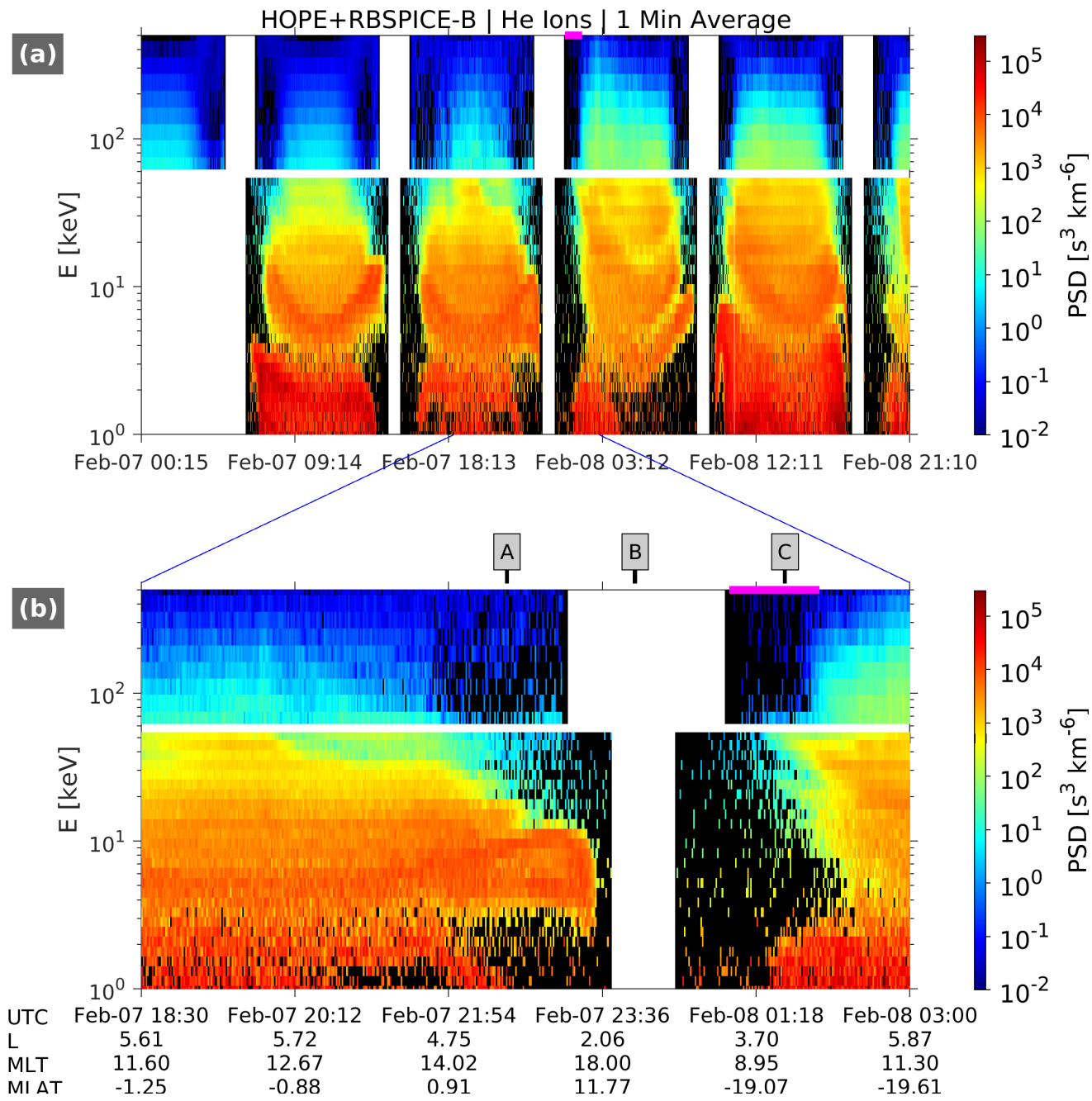
Figure S5. Proton PSD measurements from Probe A (analogous format to the figure in the manuscript).

May 3, 2021, 9:39pm

Figure S6. Oxygen PSD measurements from Probe A (analogous format to the figure in the manuscript).
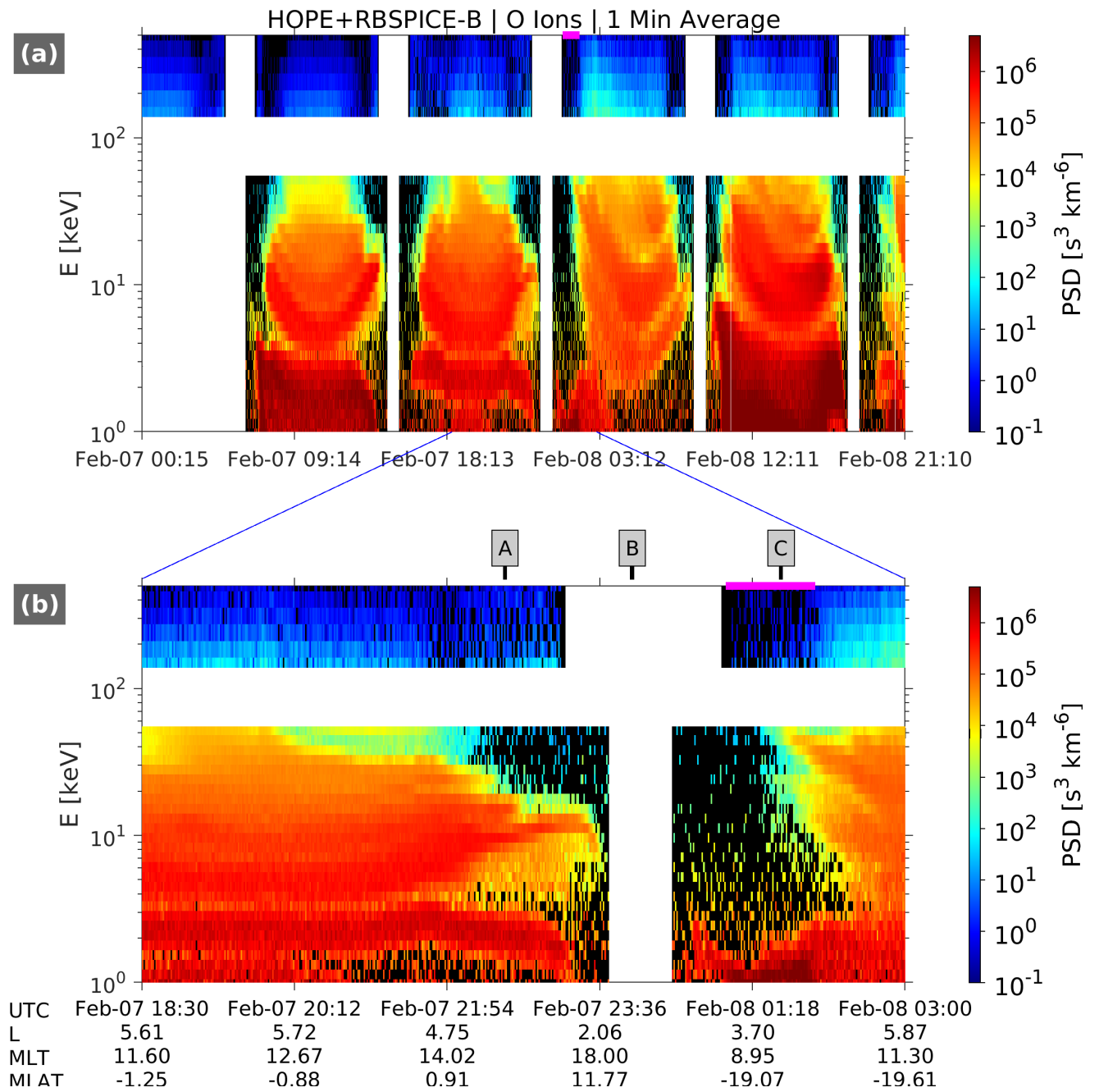
May 3, 2021, 9:39pm

Figure S7. Proton PSD measurements from Probe B (analogous format to the figure in the manuscript).

May 3, 2021, 9:39pm

Figure S8. Helium PSD measurements from Probe B (analogous format to the figure in the manuscript).

May 3, 2021, 9:39pm

Figure S9. Oxygen PSD measurements from Probe B (analogous format to the figure in the manuscript).

May 3, 2021, 9:39pm